JOURNAL OF SPACECRAFT AND ROCKETS
Vol. 38, No. 5, September–October 2001

Engineering Notes

ENGINEERING NOTES are short manuscripts describing new developments or important results of a preliminary nature. These Notes cannot exceed six manuscript pages and three figures; a page of text may be substituted for a figure and vice versa. After informal review by the editors, they may be published within a few months of the date of receipt. Style requirements are the same as for regular contributions (see inside back cover).

Practical Prediction of Supersonic Viscous Flows over Complex Configurations Using Personal Computers

Vahid Esfahanian*
University of Tehran, Tehran, Iran
Aziz Azimi†
Sharif University of Technology, Tehran, Iran
and
Kazem Hejranfar‡
University of Tehran, Tehran, Iran

Nomenclature

a	=	speed of sound
C_A	=	axial force coefficient
C_N	=	normal force coefficient
E	=	total energy per unit volume
$\boldsymbol{F}, \boldsymbol{G}, \boldsymbol{H}$	=	transformed flux vectors
J	=	geometrical Jacobian
L	=	reference length (body diameter)
M	=	Mach number
Pr	=	Prandtl number
p	=	pressure
Re_∞	=	freestream Reynolds number, $Re_\infty = \rho_\infty u_\infty L/\mu_\infty$
T	=	temperature
t	=	time
U, V, W	=	contravariant velocities in ξ, η, ζ direction
$\boldsymbol{U}$	=	solution vector, $\boldsymbol{U}^T = J^{-1}[\rho, \rho u, \rho v, \rho w, E]$
u, v, w	=	Cartesian velocities in x, y, z direction
x, y, z	=	Cartesian coordinates
γ	=	ratio of specific heats
μ	=	dynamic viscosity
ξ, η, ζ	=	computational coordinates
ρ	=	density

Subscripts

i	=	inviscid vector
l	=	laminar flow
t	=	turbulent flow
v	=	viscous vector
∞	=	freestream condition

Introduction

IN practical supersonic aerodynamic calculations for flight vehicles, the flow contains various regimes (subsonic, transonic, and supersonic), flow separation regions, and strong interaction between inviscid and viscous layers requiring the solution of the thin-layer Navier–Stokes (TLNS) equations. However, the computation of supersonic viscous flows over a complete vehicle geometry using the TLNS equations requires very high storage and computer speed, especially for turbulent flow where relatively high-resolution grid points are needed in the viscous region.

For most bodies of practical interest, there are regions of the flow for which the parabolized Navier–Stokes (PNS) equations can be used instead of the TLNS equations, which substantially reduces the computation time and memory needed. The PNS equations are a mixed set of hyperbolic–parabolic equations; therefore, for stable space marching of these equations, the inviscid outer region of the flow must be supersonic and the streamwise velocity component must be everywhere positive. Consequently, the PNS equations cannot be applied to compute the portions of the flowfield with subsonic region of blunt nose or finned region with small sweep angle that may produce the streamwise separation. However, the PNS equations can be used for computation of flowfields with crossflow separation.

For practical prediction of supersonic viscous flowfields about complex configuration, one can choose an appropriate strategy that uses the combination of the TLNS and PNS equations to reduce the computational efforts and required storage.[1] The missile configuration may be divided into multiple regions (Fig. 1). The type of equations used in each region depend on geometry and flow conditions. The nose and finned regions are solved using the TLNS equations, and the regions with small axial geometric variation are computed using the PNS equations. The initial data plane of the PNS equations for the marching procedure can be obtained from the TLNS equations, and the TLNS equations are solved using the boundary condition provided by the PNS solution. It should be noted that the PNS and TLNS zones may have two different grid distributions, which requires interpolation.

Such a strategy enables us to perform the computations of three-dimensional steady supersonic viscous turbulent flows over finned and body-alone configurations using personal computers. To demonstrate the efficiency and accuracy of the present methodology, the aerodynamic characteristics of these configurations are also obtained by the purely TLNS solution and the results are compared with those of the TLNS–PNS approach. The present computations are also compared with the experimental results.

Problem Formulation

TLNS Equations

The TLNS equations are obtained from the full Navier–Stokes equations by neglecting viscous terms associated with streamwise derivatives. These equations are applicable for flows with high Reynolds numbers (i.e., thin boundary layer). The TLNS equations

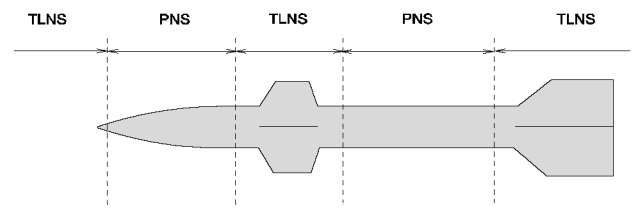

Fig. 1 Practical flow computation procedure over a typical missile configuration.

Received 30 June 2000; revision received 15 May 2001; accepted for publication 15 June 2001.

*Associate Professor, Mechanical Engineering Department, P.O. Box 11365-4563 North Amir-Abad Avenue.
†Ph.D Candidate, Mechanical Engineering Department, P.O. Box 11365-9567 Azadi Avenue.
‡Ph.D Candidate, Mechanical Engineering Department, P.O. Box 11365-4563 North Amir-Abad Avenue.

can be written in nondimensional strong conservation form in generalized coordinate system as follows:

$$\frac{\partial \boldsymbol{U}}{\partial t}+\frac{\partial \boldsymbol{F}_i}{\partial \xi}+\frac{\partial \boldsymbol{G}_i}{\partial \eta}+\frac{\partial \boldsymbol{H}_i}{\partial \zeta}=\left[\frac{\partial \boldsymbol{G}_v}{\partial \eta}+\frac{\partial \boldsymbol{H}_v}{\partial \zeta}\right] \tag{1}$$

All quantities are nondimensionalized using reference length L and freestream conditions. The numerical method is based on an efficient, noniterative, implicit, finite-difference factored algorithm of Beam and Warming[2] to solve the unsteady TLNS equations in a generalized, curvilinear coordinate system. The final steady-state solution is obtained by marching asymptotically in time. The method is second-order accurate in space and first-order accurate in time.

PNS Equations

The PNS equations are obtained by dropping the unsteady term in the TLNS equations and modifying the pressure gradient in the streamwise convective flux vector to permit stable marching. The PNS equations are

$$\frac{\partial \boldsymbol{F}_i}{\partial \xi}+\frac{\partial \boldsymbol{G}_i}{\partial \eta}+\frac{\partial \boldsymbol{H}_i}{\partial \zeta}=\left[\frac{\partial \boldsymbol{G}_v}{\partial \eta}+\frac{\partial \boldsymbol{H}_v}{\partial \zeta}\right] \tag{2}$$

The presence of the streamwise pressure gradient term in the streamwise convective flux vector permits the upstream influences to occur in the subsonic region of boundary layer, which leads to exponentially growing solutions referred to as departure solutions.[3] Several different techniques for avoiding the PNS departure behavior have been proposed to eliminate this difficulty. Stable marching of numerical solution of the PNS equations is achieved in the subsonic region of the boundary layer by using the methods proposed by Vigneron et al.[4] and Schiff and Steger.[5] Both methods are implemented in the present PNS code. For this Note, the Vigneron technique is used.

In the Vigneron approximation, the streamwise pressure gradient in the momentum equations is split into an implicit contribution and an explicit contribution:

$$\frac{\partial p}{\partial \xi}=\left[\omega\frac{\partial p}{\partial \xi}\right]_{\text{implicit}}+\left[(1-\omega)\frac{\partial p}{\partial \xi}\right]_{\text{explicit}} \tag{3}$$

The weighting function ω is determined as

$$\omega=\min\left[1,\frac{\sigma\gamma M_\xi^2}{1+(\gamma-1)M_\xi^2}\right] \tag{4}$$

where M_ξ is the Mach number in the marching direction and σ is an appropriate safety factor, typically assigned a value in the range of 0.80–0.90, to account for nonlinearities in the analysis. To introduce the Vigneron technique into the PNS equations, a new vector $\bar{\boldsymbol{F}}_i$ is defined as

$$\bar{\boldsymbol{F}}_i=\boldsymbol{F}_i-\boldsymbol{P} \tag{5}$$

Therefore, the new form of the PNS equations appears as

$$\frac{\partial \bar{\boldsymbol{F}}_i}{\partial \xi}+\frac{\partial \boldsymbol{P}}{\partial \xi}+\frac{\partial \boldsymbol{G}_i}{\partial \eta}+\frac{\partial \boldsymbol{H}_i}{\partial \zeta}=\left[\frac{\partial \boldsymbol{G}_v}{\partial \eta}+\frac{\partial \boldsymbol{H}_v}{\partial \zeta}\right] \tag{6}$$

where the inviscid vectors $\bar{\boldsymbol{F}}_i$ and $\boldsymbol{P}$ are

$$\bar{\boldsymbol{F}}_i=J^{-1}\begin{pmatrix}\rho U\\ \rho u U+\omega\xi_x p\\ \rho v U+\omega\xi_y p\\ \rho w U+\omega\xi_z p\\ (E+p)U\end{pmatrix},\qquad \boldsymbol{P}=J^{-1}\begin{pmatrix}0\\ \xi_x(1-\omega)p\\ \xi_y(1-\omega)p\\ \xi_z(1-\omega)p\\ 0\end{pmatrix}$$

In this study, the elliptic part of streamwise pressure gradient term ($\boldsymbol{P}$) responsible for upstream disturbance propagation is omitted to permit the space-marching procedure to be stable. The PNS equations in the generalized coordinate system (ξ, η, ζ) are solved by the use of the efficient, implicit, finite-difference factored algorithm of Beam and Warming[2] for a spatial marching scheme. The algorithm utilizes the first-order backward Euler implicit scheme in the marching direction (ξ) and the second-order central scheme in the wall-normal (η) and transverse directions (ζ).

Turbulence Modeling

For turbulent-flow computations, a Reynolds averaged form of the TLNS and the PNS equations is used.[1] Therefore, the dependent variables represent the mean-flow contribution. By using the Boussinesq hypothesis, turbulence modeling is reduced to evaluate the turbulent viscosity coefficient μ_t. Consequently, the Reynolds average form of the TLNS and PNS equations can be obtained by replacing the laminar flow coefficients with

$$\mu=\mu_l+\mu_t,\qquad \mu/Pr=\mu_l/Pr_l+\mu_t/Pr_t \tag{7}$$

where the coefficient of viscosity μ_l is computed by Sutherland's law, Pr_l is assumed to be constant and equal to 0.72, and a value of 0.90 is used for Pr_t. The turbulent viscosity coefficient μ_t is calculated using the well-known two-layer algebraic eddy viscosity model suggested by Baldwin and Lomax.[6]

Grid Generation

An algebraic method is utilized to generate grids in unfinned regions, and the Poisson grid generation method based on work of Hsu and Lee[7] is used to generate grids in finned regions. To have the same distribution grid points in all the regions, the grid calculated in the finned region is redistributed in each ray normal to the body using the algebraic method with the same constant clustering parameter used in the unfinned region.

Results and Discussion

The computations have been performed for supersonic flow over finned and body-alone configurations. The finned configuration consists of an ogive cylinder with four fins at the end of body. The geometry of the finned configuration and the computation strategy are shown in Fig. 2. The fins are made of plates with a thickness of 5% of the root chord. The edge of the fins is wedge formed with a 20 deg angle. The flow conditions are a freestream Mach number of $M_\infty=2.01$, a freestream unit Reynolds number of $Re_\infty/\text{m}=1.3\times10^7$, and a freestream temperature of $T_\infty=159.3$ K. The wall is assumed to be adiabatic. The flowfield over the finned configuration has been computed using three regions, namely nose, cylinder, and finned portions, using the TLNS–PNS approach. In the nose and finned regions ($30\times51\times31$) and ($40\times51\times61$) grid points have been used for the TLNS code, respectively. The PNS code has been applied for the cylinder region using (101×41) grid points with 1000 sweeps in the streamwise direction ($\Delta\xi=0.0125$).

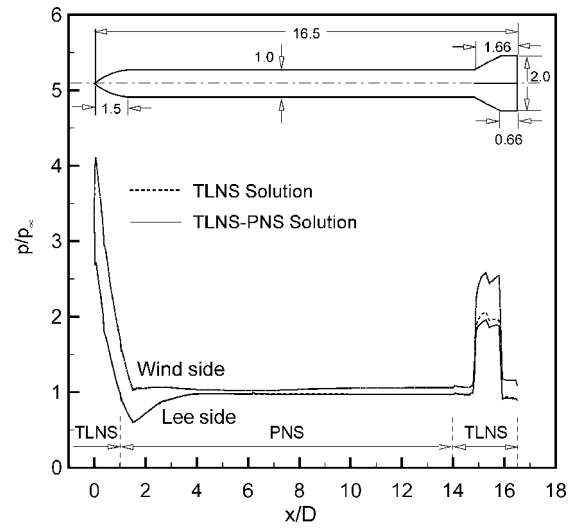

Fig. 2 Axial surface pressure distribution on wind and lee sides of finned configuration: $M_\infty=2.01$, $Re_\infty/\text{m}=1.3\times10^7$, and $\alpha=8.45$ deg.

To demonstrate the accuracy and efficiency of the TLNS–PNS approach, the computations for finned and body-alone models also have been obtained using purely the TLNS solution for two values of angle of attack. For this reason, the PNS zone is replaced by two TLNS zones. To have the same spatial accuracy, $(62 \times 101 \times 41)$ grid points are used in each TLNS zone. It should be noted that the PNS solution has the first-order spatial accuracy in the ξ direction, but the TLNS solution is the second-order spatial accuracy $[\Delta\xi_{\text{TLNS}} = \sqrt{(\Delta\xi_{\text{PNS}})} = 0.112]$. All the present calculations have been performed on 500 MHz Pentium III computer. A global root mean square of 10^{-8} has been applied as a convergence criterion for the TLNS code (using CFL = 1):

$$\text{Error} = \frac{1}{5}\frac{\left(\sum_{n=1}^{5}\sum_{i=1}^{i\,\max}\sum_{j=1}^{j\,\max}\sum_{k=1}^{k\,\max}[\Delta U]^2_{n,i,j,k}\right)^{\frac{1}{2}}}{i\,\max \times j\,\max \times k\,\max \times \Delta t_{\min}} \tag{8}$$

where $\Delta t_{\min}$ is the minimum value of Δt in the domain and the CFL number is defined as

$$\text{CFL} = \Delta t \times \lambda_{\max} \tag{9}$$

where

$$\lambda_{\max} = \text{Max}\left[U + a\sqrt{\xi_x^2 + \xi_y^2 + \xi_z^2}, V + a\sqrt{\eta_x^2 + \eta_y^2 + \eta_z^2}, W + a\sqrt{\zeta_x^2 + \zeta_y^2 + \zeta_z^2}\right] \tag{10}$$

In addition, a shock-capturing approach has been used in both the TLNS and PNS codes. The typical computation times for finned configuration have been 12 and 133 h for the TLNS–PNS and purely TLNS approaches, respectively. It is clear that the TLNS–PNS strategy significantly reduces the computational time.

Figure 2 shows the axial surface pressure distributions on the wind and lee sides at an angle of attack of 8.45 deg for the TLNS–PNS and purely TLNS approaches. The axial surface pressure distributions of the two approaches are the same in the cylinder region, and small differences exist only on the lee side of the finned region. Figure 3a shows the circumferential plane of grid and Mach contours for the finned station, $x/D = 15.92$, at an angle of attack of 8.45 deg for the TLNS–PNS approach. The orthogonality and clustering of grids near the body surface can be clearly seen. Figure 3b presents circumferential pressure contours and circumferential crossflow velocity vectors for this case. The clustered pressure contours above the fins indicate the fin shocks, and a strong crossflow separation region is evident, especially for the central fin.

Figure 4 shows the predicted aerodynamic coefficients, including the axial and normal forces at various angles of attack for finned and body-alone models. The results indicate that the aerodynamic coefficients obtained from the TLNS–PNS and purely TLNS approaches

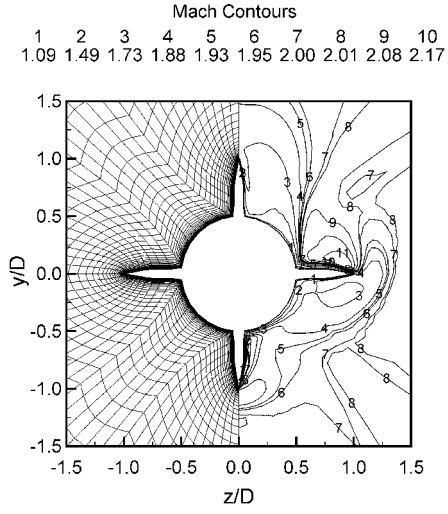

Fig. 3a Circumferential plane of grid and Mach contours.

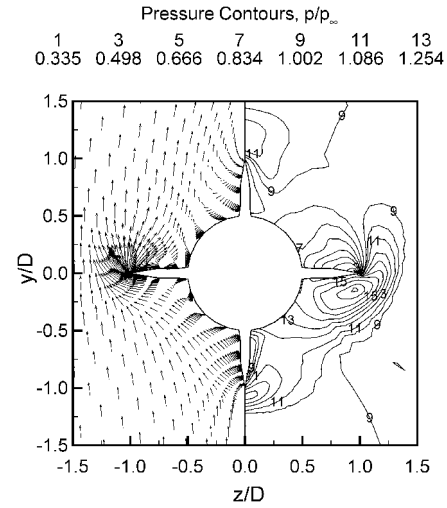

Fig. 3b Crossflow plane velocity vectors and pressure contours for finned configuration at $x/D = 15.92$, $M_\infty = 2.01$, Re_∞/m = 1.3×10^7, and $\alpha = 8.45$ deg.

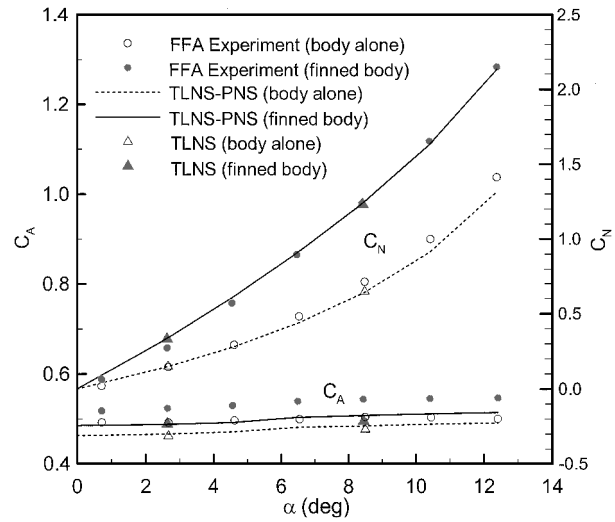

Fig. 4 Variations of axial and normal force coefficients vs angle of attack for finned and body-alone configurations: $M_\infty = 2.01$ and Re_∞/m = 1.3×10^7.

are in good agreement. In comparison with other experiments,[8] excellent agreements are obtained for the normal force coefficients and small discrepancies exist for the axial force coefficients. It can be seen that the majority of normal force comes from the body at high angles of attack.

Conclusions

The three-dimensional supersonic viscous flows over complex configurations have been computed using appropriate combinations of the TLNS and PNS equations. The calculations have been obtained for supersonic turbulent flows at high angles of attack over finned and body-alone configurations. The present computations have been compared with those of purely TLNS solution and experimental data, which show good agreement. The present study shows that the regions computed by the PNS equations can be used to provide appropriate boundary conditions to solve the TLNS equations in the next region. This Note demonstrates that the mixed TLNS–PNS algorithm significantly reduces the amounts of computation and storage needed for practical prediction of flowfield around complex geometries. Therefore, the present algorithm is very efficient (time and memory) for supersonic flowfield computations and can be performed on personal computers. However, for more robust code, the multiblock capability has to be added to the code.

Acknowledgment

The authors would like to thank the University of Tehran for financial support of this work.

References

[1]Esfahanian, V., Azimi, A., and Hejranfar, K., "Practical Prediction of Supersonic Viscous Flow over Complex Configurations," *8th Annual Conference of the Computational Fluid Dynamics Society of Canada*, Vol. 1, Computational Fluid Dynamics Society of Canada, Montreal, QC, Canada, 2000, pp. 291–299.

[2]Beam, R. M., and Warming, R. F., "An Implicit Factored Scheme for the Compressible Navier–Stokes Equation," *AIAA Journal*, Vol. 16, No. 4, 1978, pp. 393–402.

[3]Tannehill, J. C., Anderson, D. A., and Pletcher, R. H., *Computational Fluid Mechanics and Heat Transfer*, 2nd ed., McGraw–Hill, New York, 1997.

[4]Vigneron, Y. C., Rakich, J. V., and Tannehill, J. C., "Calculation of Supersonic Viscous Flow over Delta Wings with Sharp Subsonic Leading Edges," AIAA Paper 78-1137, July 1978.

[5]Schiff, L. B., and Steger, J. L., "Numerical Simulation of Steady Supersonic Viscous Flow," *AIAA Journal*, Vol. 18, No. 12, 1980, pp. 1421–1430.

[6]Baldwin, B. S., and Lomax, H., "Thin-Layer Approximation and Algebraic Model for Separated Turbulent Flow," AIAA Paper 78-257, Jan. 1978.

[7]Hsu, K., and Lee, S. L., "A Numerical Technique for Two-Dimensional Grid Generation with Grid Control at all of the Boundaries," *Journal of Computational Physics*, Vol. 96, 1991, pp. 451–469.

[8]Gudmundson, S. E., and Torngren, L. R., "Supersonic and Transonic Wind Tunnel Tests on a Slender Ogive-Cylinder Body Single and in Combination with Cruciform Wings and Tails of Different Sizes," Aeronautical Research Inst. of Sweden, Rept. FFA AU-772, Stockholm, April 1972.

R. M. Cummings
Associate Editor

Catalytic Model on SiO_2-Based Surface and Application to Real Trajectory

Takuji Kurotaki*
National Aerospace Laboratory, Tokyo 182-8522, Japan

Introduction

WHEN a reentry vehicle flies at very high Mach numbers, a strong bow shock forms in front of the body, and dissociation of air takes place inside the shock layer. Some of dissociated atoms recombine according with the drop of temperature; however, if the flow is in nonequilibrium a large part of atoms remain through the boundary layer and finally recombine on the surface, which causes the increase in aerodynamic heat.

One way to protect this additional increase of heat flux is to use the thermal protection system (TPS) with materials as little catalytic as possible. SiO_2-based materials are now widely used for this purpose because of their low catalytic properties. However, even the slight catalysis of these materials increases considerable amount of heat flux around the body compared with the one with noncatalytic wall assumption.

In the design of reentry vehicles, the heat load is usually predicted through computational fluid dynamics (CFD), and two extreme assumptions are usually applied; non- or fully catalytic conditions. Designing reentry vehicles with fully catalytic condition seems to be too conservative today because it may sometimes lead to overestimation of weight of TPS and even misunderstanding of correct aerodynamic properties.[1,2] Therefore, construction of the model describing the correct physics of heterogeneous catalytic processes and being easy to incorporate into the CFD codes are now of great importance. For this purpose several models have been proposed in which the catalytic processes are treated as the combination of each elementary step.[1–4] However, more improvements in physical considerations are necessary to predict catalytic efficiencies quantitatively for various flow conditions.

In the treatment of surface catalysis in airflow, it is usually assumed that no production of NO molecules occurs. Recently, Copeland et al.[5] demonstrated that a significant concentration of NO is generated from a surface-catalyzed reaction on quartz surfaces in the room temperature range. They also pointed out that N and O atoms do not act independently and that NO may be a significant reaction product from a catalytic process.

In this Note a model describing heterogeneous catalysis on the surface of SiO_2-based materials is constructed in a new approach. The concept of the phenomenological theory proposed by Kovalev et al.[6] are generalized to describe the overall heterogeneous catalytic phenomenon including NO production in each elementary step in detail. To prove the validity of this theory and investigate the effects of NO production on the surface, this model is incorporated into the CFD codes, the flow around OREX (Orbital Reentry Experiment) is solved, and results are discussed.

Description of Heterogeneous Catalysis and Construction of Model

In this Note the following elementary steps are assumed in heterogeneous catalytic processes under the assumption that the surface temperature is not extremely high and that there are no slip effects.

1) Adsorption-desorption of atoms:

$$\mathrm{O} + (\mathrm{S}) \rightleftharpoons (\mathrm{O}-\mathrm{S}) \tag{1}$$

$$\mathrm{N} + (\mathrm{S}) \rightleftharpoons (\mathrm{N}-\mathrm{S}) \tag{2}$$

2) Recombination between gas atoms and adsorbed atoms (adatoms) [Eley–Rideal (E-R) recombination]:

$$\mathrm{O} + (\mathrm{O}-\mathrm{S}) \rightleftharpoons \mathrm{O_2} + (\mathrm{S}) \tag{3}$$

$$\mathrm{N} + (\mathrm{N}-\mathrm{S}) \rightleftharpoons \mathrm{N_2} + (\mathrm{S}) \tag{4}$$

$$\mathrm{O} + (\mathrm{N}-\mathrm{S}) \rightleftharpoons \mathrm{NO} + (\mathrm{S}) \tag{3'}$$

$$\mathrm{N} + (\mathrm{O}-\mathrm{S}) \rightleftharpoons \mathrm{NO} + (\mathrm{S}) \tag{4'}$$

3) Recombination between adatoms [Langmuir–Hinshelwood (L-H) recombination]:

$$(\mathrm{O}-\mathrm{S})_m + (\mathrm{O}-\mathrm{S}) \rightleftharpoons \mathrm{O_2} + 2(\mathrm{S}) \tag{5}$$

$$(\mathrm{N}-\mathrm{S})_m + (\mathrm{N}-\mathrm{S}) \rightleftharpoons \mathrm{N_2} + 2(\mathrm{S}) \tag{6}$$

$$(\mathrm{O}-\mathrm{S})_m + (\mathrm{N}-\mathrm{S}) \rightleftharpoons \mathrm{NO} + 2(\mathrm{S}) \tag{5'}$$

$$(\mathrm{N}-\mathrm{S})_m + (\mathrm{O}-\mathrm{S}) \rightleftharpoons \mathrm{NO} + 2(\mathrm{S}) \tag{6'}$$

Here (S) is a free active site and (Y–S) means an Y atom absorbed by the surface (adatom). The subscript m means migrating adatoms on the catalytic surface.

In L-H recombination only collisions between this migrating adatom and a "still adatom" are considered.[2] Furthermore, adsorption–desorption of molecules in the wall temperature range considered in this study is sufficiently small and can be neglected.[6] Under these assumptions the specific mass formation rates $\dot{r}_s$ per unit surface area in reactions Eqs. (1–6) and Eqs. (3′–6′) are given from the acting surface law by[6]

$$\dot{r}_1(\mathrm{O}) = -\dot{r}_1(\mathrm{O}-\mathrm{S}) = -M_O p k_1 (X_O \theta - \theta_O / p K_1), \qquad \text{etc.} \tag{7}$$

under the condition that

$$\theta + \theta_O + \theta_N = 1 \tag{8}$$

Presented as Paper 2000-2366 at the AIAA 34th Thermophysics Conference, Denver, CO, 19–22 June 2000; received 10 August 2000; revision received 24 April 2001; accepted for publication 30 April 2001.

*Senior Researcher, Fluid Science Research Center, Chofu; kurotaki@nal.go.jp. Member AIAA.